ELSEVIER

Contents lists available at ScienceDirect

Journal of Non-Crystalline Solids

journal homepage: www.elsevier.com/locate/jnoncrysol





Rheology of an alkali-activated Fe-rich slag suspension: Identifying the impact of the activator chemistry and slag particle interactions

Glenn Beersaerts ^{a,*}, Anja Vananroye ^b, Dimitrios Sakellariou ^c, Christian Clasen ^b, Yiannis Pontikes ^a

- ^a KU Leuven Department of Materials Engineering, Kasteelpark Arenberg 44-bus 2450, Heverlee 3001, Belgium
- ^b KU Leuven Department of Chemical Engineering, Celestijnenlaan 200f-bus 2424, Heverlee 3001, Belgium
- ^c KU Leuven Department of Microbial and Molecular Systems (M²S), Celestijnenlaan 200f–bus 2461, Heverlee 3001, Belgium

ARTICLE INFO

Keywords: Rheology Elastic moduli Elastic properties Alkali activated cement Glass Amorphous material

ABSTRACT

Iron-silicate slags, originating from metallurgical industry, are upon alkali-activation precursors for synthesis of inorganic polymer binders, which can be used in construction. The slag's rheology is important for certain construction applications, which is for alkali-activated Fe-rich slag suspensions (AAS) still largely unmapped. To identify the contribution of the activator and of an early formed binder to the rheology, the activator SiO_2/Na_2O molar ratio and SiO_2/Na_2O molar ratio and H2O content was modified. The flow behaviour of AAS was compared with an activator alone, and a quartz suspension to reveal the effect of the slag particles on the rheology and its degree of activation. Raising SiO_2/Na_2O molar ratio resulted in a higher yield stress and elasticity, explained by the increase of silicate complexes, while decreasing SiO_2/Na_2O molar ratio resulted in more monomers. AAS exhibited a yield stress fluid-like behaviour conform to the Herschel-Bulkley model and driven by the strong physical interaction between the slag particles.

1. Introduction

Pyrometallurgical production of non-ferrous metals is accompanied by the generation of substantial volumes of Fe-rich slags. From these slags, consisting of mainly Fe₂O₃, SiO₂ and Al₂O₃, an inorganic polymer (IP) binder can be formed after alkali-activation. This IP binder can be suitable for building materials, which can be more environmental friendly compared to ordinary Portland cement (OPC) based binders. The choice of the activating solution plays a major role in the slag activation potential [1]. Once the slag particles are introduced to an activating solution, which is in most cases an alkali-silicate solution, the particles are partially dissolved, and once a saturation threshold is reached, polymerization of Fe, Al, Si, and Na species can take place [2-4] and an amorphous densely crosslinked IP binder is formed. The microstructure, reactivity, and mechanical performances of IPs have been investigated in a number of studies [1,5,6], but the rheological properties, prior to the formation of an IP binder, have not. However, the rheology of a slag-based suspension before polymerising is important, in particular for any flow-related application in construction, such self-levelling. Further, the effect of the alkali-silicate chemistry and the slag particle interaction potential on the rheological behaviour of a slag suspension is not investigated so far. In order to increase the slag valorisation potential towards IPs, the rheology of alkali-activated slag suspensions needs to be investigated.

According to existing literature, a liquid geopolymer paste, similar to IPs, can be identified before hardening as a suspension that consists of three phases: the alkali-silicate solution, the early formed binder, and the undissolved fraction of the precursor particles [7,8]. These three phases contribute to the viscosity and yielding behaviour of the fresh paste [9]. The yielding and viscosity are primarily controlled by the H₂O amount [10–15] and the SiO₂ to Na₂O ratio in the activating solution [16]. Furthermore, the ionic concentration of the activator, the particle interaction potential (Van der Waals, electrostatic and steric forces), the particle surface potential, the particle shape, and the grading of the precursor particles influences viscosity and yield stress as well [11,17, 18]. The yield strain depends on the suspension composition and is different for an IP paste [1] compared to an ordinary Portland cement (OPC) based paste [19]. However, there are generally different

E-mail addresses: glenn.beersaerts@kuleuven.be (G. Beersaerts), anja.vanaroye@kuleuven.be (A. Vananroye), dimitrios.sakellariou@kuleuven.be (D. Sakellariou), christian.clasen@kuleuven.be (C. Clasen), yiannis.pontikes@kuleuven.be (Y. Pontikes).

^{*} Corresponding author.

procedures described in literature that deliver different values for the onset stress of flow, resulting in no clear definition on yield stress [13, 20].

The rheological behaviour of binder systems other than IP pastes has been studied extensively, but those results cannot be directly translated to IP pastes as the precursor chemistry can differ significantly, and thus it is important to investigate and understand their specific rheological properties. An OPC based suspension is reported to exhibit a viscoelastic behaviour [11,12] with shear thinning characteristics [21]. Suspensions from blended cements are more closely related to IP pastes and exhibit a lower yield stress when a higher slag to cement ratio is used [22]. Depending on the slag, the rheological behaviour of the suspension can be described using constitutive models that incorporate yield stress. Na-silicate activated ground granulated blast furnace slag has a lower yield stress in comparison to an OPC based paste, but can be described by the Herschel-Bulkley model, while the OPC based pastes can be described by a Bingham model [16]. The Herschel-Bulkley model, however, is better suited to predict the behaviour of fly ash geopolymers [23]. Favier et al. (2013) mention that a metakaolin-based geopolymer paste shows no flocculation and does not exhibit a yield stress. They concluded that such a geopolymer paste exhibits a Newtonian behaviour, controlled by the high viscosity of the sodium silicate solution [21]. However, other studies have shown that silicates in the activating solution can have a physical effect on the particles, increasing the yield stress and enhancing the observed shear thinning [24]. The contribution of the Newtonian alkali-silicate solution to the viscosity and yielding properties can be related to its molecular structure and the H₂O volume fraction [21]. The aforementioned literature indicates that the activating solution chemistry, in combination with the choice of the solid precursor, plays an important role in the rheological properties.

This paper addresses the gap in understanding the rheological behaviour of an alkali-activated Fe-rich slag suspension and to which extend the slag, activating solution or a possible early formed binder contributes to the rheological behaviour. The physical effect of different activating solution chemistries on the slag suspension is investigated by both oscillatory and rotational rheology. Oscillatory rheology provides insights into the viscoelastic properties via the storage modulus G' and loss modulus G" at specific frequencies and strains, where G' is a measure for the elastic part and G" is related to the viscous contribution of the suspension [11]. The yield strain or linear strain amplitude was determined for each paste by strain amplitude sweeps at fixed frequencies. Angular frequency sweeps, at a constant strain amplitude in the linear viscoelastic (LVE) regime, were performed to investigate the extent of structural organization in the suspension from the elastic response of the suspension at higher frequencies. Steady rotational measurements provide insights into viscosity and stress changes as a function of time or flow rate. Shear rate sweeps provided information on the yield stress and shear thinning. A comparative study with an inert quartz suspension is performed to identify the significance of the attractive interparticle forces and interaction between the slag particles. Based on the obtained rotational data, the rheological behaviour of the paste or suspension was linked to and fitted by the corresponding constitutive model.

2. Material and methods

2.1. Slag precursor and quartz analysis

The slag originated from the recycling and refinement of non-ferrous metals, such as Pb and Cu waste. The bulk composition of the Fe-rich slag was analyzed by X-Ray Fluorescence (XRF, PW 2400, Philips). The chemical composition of the slag is shown in Table 1. The crystalline composition of the slag was analyzed by X-Ray Diffraction (D2 phaser XRD, Bruker). The XRD analysis indicated that the slag was 78 wt% amorphous and consisted of fayalite (18 wt%), hercynite (3 wt%), magnetite (<1 wt%), and zincite (<1 wt%) minerals. The chemical and

Table 1
The chemical bulk composition of the Cu-slag expressed in weight percent.

FeO	SiO_2	ZnO	Al_2O_3	Na ₂ O	CaO	Others
52.5	26.2	7.7	4.6	2.7	1.2	5.1

mineralogical composition is comparable to previous works [1].

Prior to the rheological measurements, the slag was milled (Attritor 1S, Wiener) to a specific particle size distribution (PSD). A maximum particle size of 100 µm was chosen to be at least one order of magnitude smaller than the dimension of the gap size between the vane blade and the cup of the rheological measurement geometry. This avoided any direct friction between the agglomerated particles and the shearing geometry. A similar milling procedure was performed for the quartz powder. After milling, the slag and quartz were sieved with a 415 μ m sieve size and a PSD analysis was performed (Malvern Mastersizer) to verify that the larger particles were excluded. The D_{10} , D_{50} , and D_{90} of the slag after milling, determined from the laser diffraction PSD analyses, equalled to 1.3 $\mu m,\,6.8~\mu m,$ and 24 $\mu m,$ respectively. The $D_{10},\,D_{50}$ and D_{90} of the quartz powder is 1.1 μ m, 11.3 μ m and 41.4 μ m, respectively. The morphology (angularity, shape) of the quartz particles and the PSD resemble to the slag particles. The PSD analyses showed that the maximum particle size was less than 100 μm and therefore suitable for the rheology measurements.

2.2. Activating solution chemistry

The sodium silicate solutions were prepared at least 24 h prior to the experiment. NaOH pellets were added to a starting solution (3.3 SiO₂/ Na₂O molar ratio and 61 wt% H₂O from Silmaco), to prepare solutions with SiO₂/Na₂O molar ratios of 1.4, 1.6, 1.8, and 2.0 (1.4-65, 1.6-65, 1.8-65, 2.0-65). Each of these solutions consisted of 65 wt% H2O, and 35 wt% Na₂O and SiO₂. Furthermore, solutions were prepared with a SiO₂/Na₂O molar ratio of 1.6 and H₂O/Na₂O molar ratios of 12.6 (59 wt % H₂O), 16.3 (65 wt% H₂O), and 20.5 (70 wt% H₂O) (1.6-59, 1.6-65, 1.6-70). A constant solution to slag mass ratio of 0.4 was used to subsequently produce the slag suspensions (paste). Once the powder was added to the activator, the suspension was mixed manually, using a spatula, for 4 min. The quartz suspension was prepared in a similar way as the slag suspension, in which an activating solution was used with a SiO_2/Na_2O molar ratio of 1.6 and 65 wt% H_2O . In order to have a mixture comparable to the slag suspension with respect to its rheological behaviour, the volume fraction of quartz was kept the same as the slag volume fraction (65.2 %). Taking the density differences into account, with the Fe-rich slag having a density of 3.9 g/cm³, while quartz powder has a density of 2.65 g/cm³, this resulted in a solution to quartz mass ratio of 0.59. Demineralised water based quartz and slag suspensions were also investigated to rule out the effect of the alkali silicate solution and the slag dissolution on the rheology. These water suspensions were prepared with the same solids volume fraction (65.2 %).

2.3. Rheology measurements

A stress-controlled rheometer (Discovery HR-3, TA Instruments) was used with a 4-bladed vane impeller (42 mm high and 28 mm diameter) in a cup (30.3 mm diameter) at a fixed temperature of 20°C and 50 % relative humidity. The suspension was loaded in the cup and, prior to each measurement, a rotational preconditioning step was performed for 200 s at an apparent shear rate of 100 1/s to guarantee similar starting conditions for each experiment. The rheological experiments were performed with a 20 min rest period after the preconditioning step, to ensure a full recovery of the suspension. The measurements lasted a maximum of 1 h after the start of mixing. Frequency and strain sweeps were performed with oscillatory shearing under controlled strain and frequency conditions to obtain the suspension storage (G') and loss (G'') modulus evolution. During a strain sweep, the strain (γ) increased

stepwise from 0.001 to 10 % with 5 pts/decade at a fixed frequency of 5 rad/s. The critical or linear strain limit was determined as the strain at which the moduli started to deviate from a constant value. During a frequency sweep, the frequency was varied stepwise from 100 to 0.1 rad/s with 5 pts/decade under a fixed γ of 0.01 %, which is situated in the prior determined linear regime.

A flow sweep was performed with a stepwise increase in \dot{y} from 0.01 to 100 1/s. The stress (σ) and viscosity (μ) data conformed to the Herschel-Bulkley constitutive models given in Eqs. (1) and (2).

$$\sigma = k\dot{y}^n + \sigma_0 \tag{1}$$

$$\mu = k\dot{y}^{n-1} + \sigma_0/\dot{y} \tag{2}$$

To fit the model to the data and to obtain the three unknown parameters, namely, the consistency index k, the flow index n, and the yield stress σ_0 , a Sum Squared Error (SSE) method was performed with the measured and calculated (optimized) data points using the Solver function in Microsoft Excel.

To determine eventual time-dependent structural changes in the suspension after the precondition, which could affect the rheological measurements, a time sweep of 1 h was performed, on the suspensions with a SiO₂/Na₂O molar ratio of 1.4 and 2.0, and the suspensions with 70 and 59 wt% $\rm H_2O$, to measure G' with a deformation γ of 0.01 % and a frequency of 5 rad/s.

2.4. Fourier transform infrared spectroscopy (ATR-FTIR)

An ALPHA 2 FTIR spectrometer (Bruker) was used to obtain an *in-situ* FTIR spectrum at room temperature for each activating solution. Prior to each test, the background was measured. Each solution was measured at least twice to determine repeatability. The spectra were analysed in the reflectance transmission mode with a resolution of 2 cm $^{-1}$. The analysed region is situated between 1200 and 800 cm $^{-1}$.

2.5. Nuclear magnetic resonance (NMR) spectroscopy of ²⁹Si

A Bruker Avance II 600 MHz standard bore NMR spectrometer equipped with a 5 mm liquid-state BBO probe was used to record 1D ²⁹Si NMR spectra. The samples were loaded in borosilicate 5 mm NMR tubes and measured at room temperature. A one-pulse sequence was implemented using 100 W and 9.0 µs for the length of the pulse, which was calibrated for $\pi/2$ flip angle. Longitudinal relaxation times (T₁) were checked and found to be less than 200 ms due to paramagnetic impurities. This is compatible with the observation of a residual line-width of 25 Hz in the ¹H NMR spectra after extensive shimming. 4096 transients were summed to produce each spectrum in 1h 7min. Exponential apodization of 5 Hz was applied to all spectra before FFT and phase correction. Silicon background signals were recorded from the probe and an empty NMR tube in the same experimental conditions (number of scans, repetitions, delays etc.) as for the samples. These signals showed weak but broad silicon lines around the Q⁴ region, as expected. The spectra were processed and the background signal was subtracted. No additional baseline correction was applied. The ²⁹Si chemical shift scale was calibrated by spiking the solutions with traces of 3-(Trimethylsilyl)propionic-2,2,3,3-d4 acid sodium salt.

2.6. Heat flow measured by calorimetry and solution chemistry by ICP-OES

The reaction kinetics of each different suspension chemistry were investigated using an isothermal calorimeter at 20°C (TAM Air, TA Instruments), right after the manual mixing step. The concentration of dissolved species in the suspension with as activator a $\text{SiO}_2/\text{Na}_2\text{O}$ molar ratio of 1.4 and 65 wt% H₂O were measured by inductively coupled plasma atomic emission spectroscopy (ICP-OES). The solution extracted

from the suspension was centrifuged 1 h after mixing for 10 min at 8000 rpm. The centrifuged solution was filtered with a 0.45 μm filter, from which 150 μl was extracted and diluted with Milli-Q water (ISO 3696). The activating solution (1.4 SiO $_2/Na_2O$ ratio and 65 wt% H $_2O$ solution) was used for background correction. The concentration of Na, Al, Si, Zn, Fe species was measured and presented in g/L.

3. Results and discussion

3.1. Alkali silicate solution characterization

The rheological behaviour of the alkali-silicate solution, prior to the addition of solid particles, shows the behaviour of a simple Newtonian liquid. The flow sweep test shows (Fig. 1) that the viscosity remains constant at 0.018 Pa.s for all shear rates and that the stress increases with a slope of 1 when increasing the shear rate. A viscosity independent from the shear rate implies that the alkali-silicates are fully dissolved. A reported possible formation of colloidal Na-Si-O-H complexes on the order of 0.6 nm size, which can form aggregates of few nm [18], is at least so small at this concentration that it is not affecting the apparent Newtonian flow behaviour in Fig. 1.

An ATR-FTIR spectra analysis was performed on the activating solutions to investigate the difference in silicate bond types or molecular structure [8]. The ATR-FTIR spectra display the relative proportion of transmission at a specific wavenumber in the silicate bonding region [25]. The transmission intensity in the silicate bonding region (1200-800 cm⁻¹) can be correlated to the proportion of tetrahedron silicon sites containing non bridging oxygens (NBO). The amount of NBO per silicon site is linked to the structural unit Qⁿ, with n varying from 0 to 4 and indicating the level of crosslinks in the silicate network [26–28]. The breadth and intensity of the Si-O-Si band in the 850-1200 cm⁻¹ region is the result of overlapping of each Qⁿ present in the activating solution [28]. The transmission band around 900-850 cm⁻¹ is related to monomeric SiO⁻ (M⁺) small anion units [29], as shown in Fig. 2A, and has little variance for different SiO₂/Na₂O molar ratios. When decreasing the SiO₂/Na₂O molar ratio, an increase in transmission intensity is visible in the 950-910 cm⁻¹ region, which is related to the increase of monomer Q0 and dimer Q1 structural units, which are tetrahedral silicates with 4 and 3 NBO, respectively [28,29]. In Fig. 2A, a peak in transmission values is visible for each activating solution in the $1000-960 \,\mathrm{cm}^{-1}$ region, which is related to the linear Q^1 [29]. A decrease of the SiO₂/Na₂O molar ratio resulted in a shift of the Si-O-Si stretching band to lower wavenumbers. The latter is related to silicates with an increased number of NBO sites and corresponds to the increased formation of monomers and dimers in the solution [28]. The Q^0 and Q^1 FTIR data for the different SiO₂/Na₂O molar ratios is supported by FTIR data from literature [28,29] and ²⁹Si NMR [30].

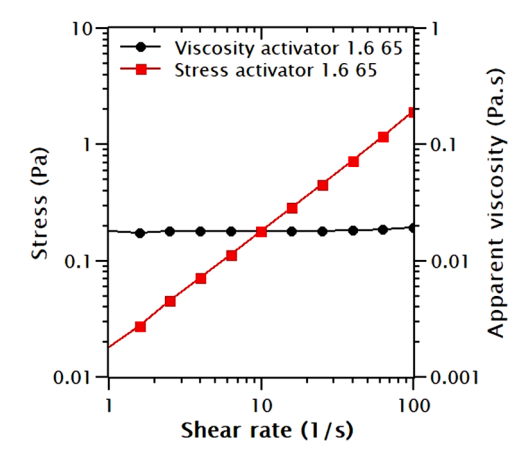


Fig. 1. The stress and viscosity of the alkali solution when increasing the shear rate.

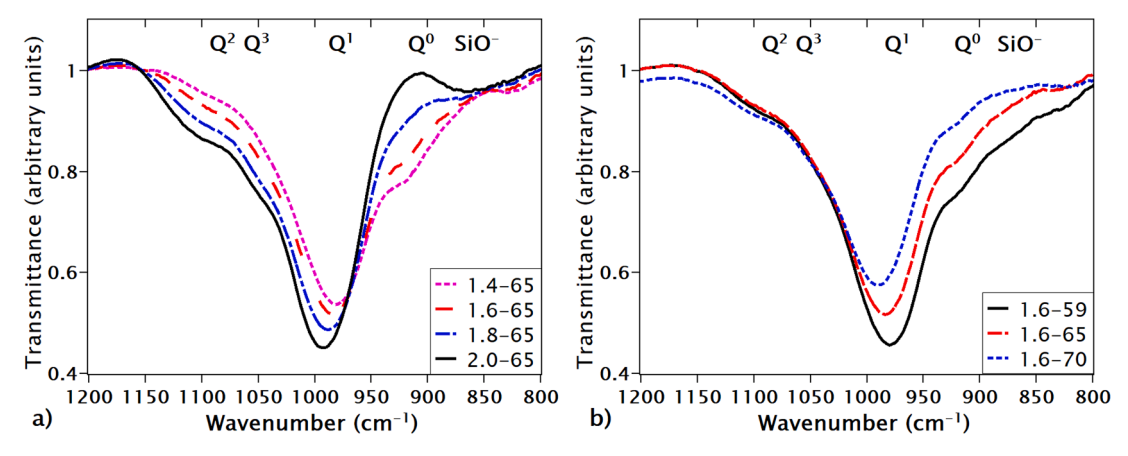


Fig. 2. The ATR-FTIR transmission spectra from 1200 to 800 cm⁻¹ of the activating solutions with different SiO_2/Na_2O ratios, indicating the $Q^{0.3}$ structural units and the Si-O-Si stretching band in (A). Fig. 2B shows the ATR-FTIR spectra of the activating solutions with different H₂O ratios.

An increase of the SiO2/Na2O molar ratio shows a shift to lower wavenumbers in the 1150-980 cm⁻¹ region, which is linked to the Q² and Q³ units, representing trimers and polymerised species. Q² (3R and 4R) units can have linear trimers, tetramers, and cyclic silicate structures containing 2 NBO and corresponds to the 1070-1030 \mbox{cm}^{-1} region [29]. Q³ (3R and 4R) units are situated in the 1120-1030 cm⁻¹ region and indicate the presence of extended silicate 3D network rings with silicates of only one NBO [28,29]. The intensity decrease of Q³ when the SiO₂/Na₂O molar ratio decreased [31] can be related to the pH or the amount of OH-, which can function as a network modifier [32]. Introducing hydroxide ions can lead to deprotonation reactions that depolymerize the silicates by dissociating the Si-O-Si bonds [28,32]. According to Bass & Turner [29], Q4 units can only occur when the SiO_2/Na_2O molar ratio is larger than 2.0. Fig. 2B illustrates that the Si-O-Si stretching band in the 850-1200 cm $^{-1}$ region becomes broader when the amount of H₂O decreases in the activating solution. A decrease in H₂O amount resulted in the presence of more silicates in the solution and, consequently, a stronger transmittance band is visible in the 985 ${\rm cm}^{-1}$ range. Fig. 2B shows a shift to lower wavenumbers in the 980-850 cm⁻¹ region when decreasing the amount of H₂O in the solution, indicating a decrease of monomers in the solution. The aforementioned shift can be explained by the fact that an increase in H2O can result in hydrolysis of monomers and, along with the small SiO anions, the formation of silanol groups, as shown in Eq. (3) [28].

$$SiO^{-}Na^{+} + H_{2}O = SiOH^{0} + Na^{+} + OH^{-}$$
 (3)

Fig. 2B illustrates that the 1050-1100 cm⁻¹ transmission band does not show a shift in wavenumbers. The structural Q^2 and Q^3 units are

similar for all solutions, indicating that no change in the extended silicate network can be expected.

²⁹Si NMR experiments were executed to support the FTIR data and the spectra are shown in Fig. 3A and B. Different Si-O bond structures can be identified in the various activating solutions on liquid-state ²⁹Si NMR spectra. The assignment of some peaks is still unclear in the existing literature. Engelhardt et al. identified the main peaks in order to obtain a general trend [33]. According to their study, the following peaks can be assigned to a particular Si-O bond: Q⁰ at -72 ppm; Q¹ at -79 ppm; cyclic trimer Q^2 at -82 ppm; Q^2 and three-ringed silicate $Q_{(3R)}^3$ from -87 to -91 ppm; four-ringed silicate $Q_{(4R)}^3$ from -96 to -98 ppm; and Q^4 at -108 ppm [34]. All solutions have three distinct groups of peaks around -72.9, -80.5, and -82.7 ppm. These peaks are identified as the monomer Q⁰ species, the dimer and linear tetramer Q¹ species, and the cyclic trimer Q^2 species, respectively [29,33]. The relative intensity of these peaks at higher ppm increased and shifted towards a higher ppm range when decreasing the SiO₂/Na₂O molar ratio in the activating solution (Fig. 3A). The peaks situated in the spectra from -87.7 ppm up to -92.0 ppm are identified as the Q^2 species and cyclic tetramers $Q^3_{(3R)}$. The peaks from -96 ppm up to -98.6 ppm are identified as tricyclic hexamers and four ringed silicates $Q_{(4R)}^3$. No visible Q^4 species were observed in accordance with the previous observations for ratios higher than or equal to 2 [35]. The relative intensity of these peaks increases gradually with increasing SiO₂/Na₂O molar ratio (Fig. 3A). This increase indicates that less silica monomers, dimers, and trimers, and more silica tetramers and hexamers are present in the solution when increasing the SiO₂/-Na₂O molar ratio, which agrees with FTIR data. In Fig. 3B, however, the

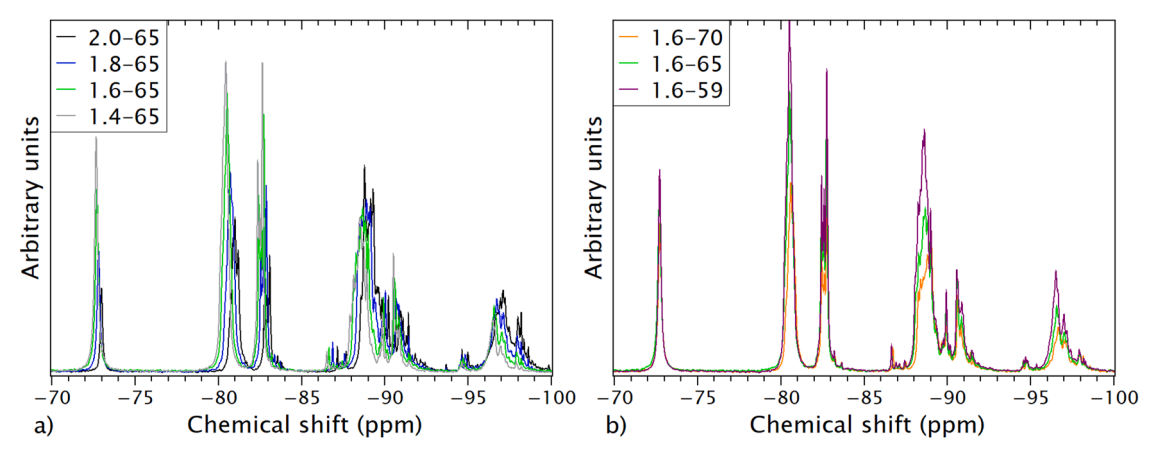


Fig. 3. The NMR pattern of the activating solutions with different SiO₂/Na₂O molar ratios in (A) and different water ratios in (B).

lowest water percentage in the activating solution has consistently higher peaks, which is related to the concentration of sodium silicates. The monomer peak shows a small change in intensity relative to concentration.

3.2. Effect of an early formed binder

The calorimetry results show that a heat flow peak is generated when the liquid is introduced to the powder. This peak can be explained as the heat released by wetting and dissolution of the particles. Once the particles are wet, the heat flow decreases to a value lower than 1 mW/g_{slag}. After this decrease, no major heat flow increase was measured for any suspension during the one hour measurement, apart from the one made with a 1.4 SiO₂/Na₂O ratio and 65 wt% H₂O solution, which shows a steady increase in heat flow (Fig. 4A). The time sweeps show an increase of the elastic modulus G' (Fig. 4B) in all suspensions, 10 min after the end of the mixing. This increase is the result of the suspension recovering from mixing and the conditioning shear step and the formation of a stable structure. After another 10 min of modulus increase, the G' value remains constant for the remainder of the 1 h measurement time window, indicating that no further structural changes take place in the suspension. The calorimetry and modulus time sweep show that during the 1st h time window post mixing, after 20 minutes no significant change in the material properties was observed, indicating that no significant amount of binder was precipitated that could affect the rheological behaviour.

The IPC-OES results from the activating solution and the centrifuged solution of the suspension with a SiO₂/Na₂O molar ratio of 1.4 and 65 wt % H₂O are shown in Table 2. The activating solution is used as a reference to the centrifuged solution and shows, as expected, a significant concentration of Na and Si. The centrifuged solution still has high concentrations for Na and Si, i.e. 147.619 and 101.473 g/L, respectively. The centrifuged solution is coloured yellow, which indicate the presence of dissolved Fe species (9 g/L). The SiO2/Na2O molar ratio of the centrifuged solution insignificantly increased by 0.05 g/L, in comparison to the activating solution. The concentration of Al, Ca, Fe and Zn is increased compared to the concentration in the activating solution but insignificant compared to the Na and Si concentrations. The abovementioned calorimetry, stiffness and ICP-OES results can imply that no significant time-dependent structural changes in the suspensions took place the 1st h post mixing, and thus no significant amount of binder phases were formed, which could affect the rheological measurements. Also the ATR-FTIR and ²⁹Si NMR measurements performed on the different activating solutions, to investigate the different bond types, are therefore representative for the suspensions.

Table 2 The concentration (g/L) of the main dissolved species in the activating solution (SiO_2/Na_2O 1.4 and 65 wt% H_2O) and the centrifuged solution from the suspension made with SiO_2/Na_2O 1.4 and 65 wt% H_2O .

g/L	Al	Ca	Fe	Zn	Na	Si
Activating solution	0.12	0.01	0.02	0.01	136.12	89.96
Centrifuged solution	2.05	0.99	9.55	0.93	147.62	101.47

3.3. Identification of the critical yield strain

The evolution of G' and G" is measured as a function of strain (from 0.001 to 10 %) to assess the deformability and to determine the yield point of the suspension. As long as G' and G" are independent of γ (Fig. 5A and B), the suspensions deformation is situated in the (LVE) response regime [24]. In this regime the suspension structure, likely related to a flocculation of the particles, is only linearly stretched under the applied deformation, and has not reached a non-linear response regime or are not even disrupted [24]. The critical strain limit of the LVE response regime is in our case determined as the strain at which the G' value deviated more than 10 % from the linear regime value [13].

As shown in Table 3 and Fig. 5A, the critical strain is independent of the SiO2/Na2O molar ratio at low ratios. A higher critical strain is obtained when using an activating solution with a SiO₂/Na₂O molar ratio above 1.6. The dependency of moduli and critical strain limit on water content (Fig. 5B) is less pronounced. The critical strain of the suspension, which was around 0.01 % (Table 3), was independent of the water content in the activating solution. The suspension with activator 70 wt% H₂O had a more pronounced G' decline in the non-linear regime beyond the critical strain in comparison to the other suspensions, which is generally understood to result from lowering the solid fraction for systems with weak forces between the particles [24] and the presence of silanol groups (Fig. 2B) with weak interactions,. The latter are easily broken down at larger γ . The results indicate that the critical strain is determined by the activating solution chemistry, while the decrease in G' is related to the particle interaction forces, which is weaker when the water volume fraction is increased.

Fig. 5C and D show the evolution of the maximum stress during an oscillation cycle with increasing strain amplitude. At low strain amplitudes, the stress increased linearly in a double logarithmic presentation with a slope of approximately 1. Eventually, at around a strain of $\sim 0.8\,$ %, a transition is visible to a stress plateau, or even a maximum, beyond which the stress declines with strain amplitude. During the initial stress increase, the suspension responds linearly to the strain and the suspension structure is not yet broken [20]. However, when the stress reaches the observed maximum, the yield stress is obtained. A further increase of strain amplitude beyond the yield stress results in disruption of the suspension structure, with the number of disrupted flocs increasing with the strain in the constant stress regime. Clearly, the

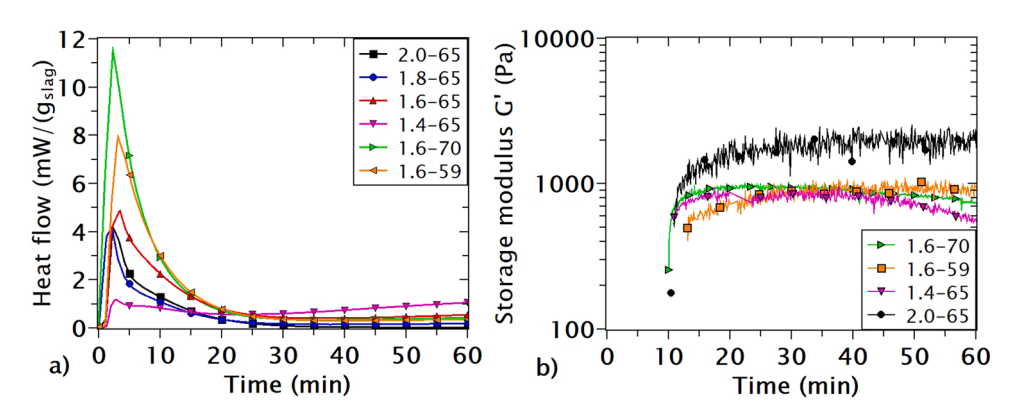


Fig. 4. The heat flow development with time for the different suspensions in (A). Fig. 4(B) presents the structural changes with time for the suspensions with a 1.4 and $2.0 \text{ SiO}_2/\text{Na}_2\text{O}$ molar ratio and a $\text{SiO}_2/\text{Na}_2\text{O}$ molar ratio with 59 and 70 wt% H₂O.

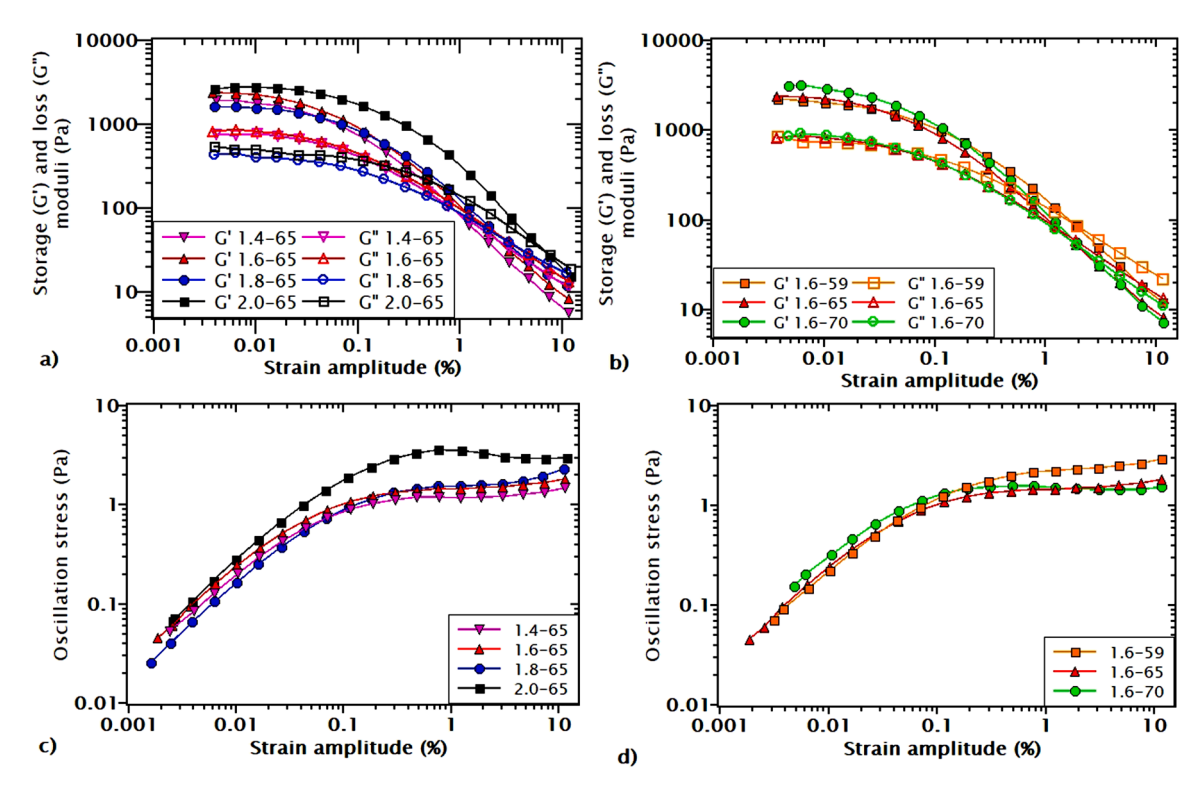


Fig. 5. The evolution of G' and G' when performing a strain amplitude sweep at a frequency of 5 rad/s for samples with different SiO₂/Na₂O ratios in (A) and H₂O amounts in (B). Panels (C) and (D) presents the evolution of oscillation stress with strain amplitude for suspensions with different SiO₂/Na₂O ratios and H₂O amounts.

Table 3The critical strain of the LVE regime for each slag suspension made from a different activating solution.

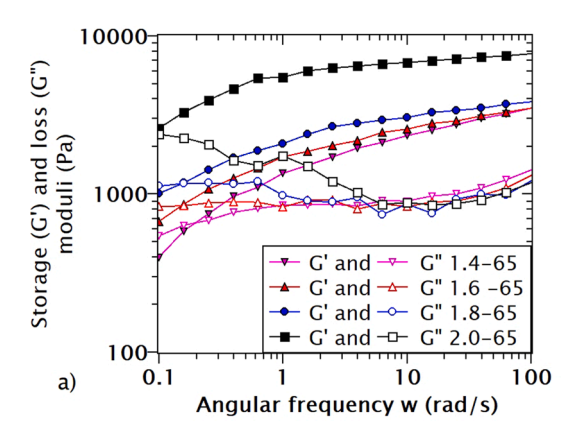
SiO ₂ /Na ₂ O ratio	1.6	1.6	1.4	1.6	1.8	2.0
H ₂ O (wt%)	59	70	65	65	65	65
Critical yield strain (%)	0.010	0.011	0.010	0.010	0.016	0.026

suspension with a $2.0~SiO_2/Na_2O$ molar ratio achieves a higher stress level before structural breakdown (Fig. 5C), indicating that this suspension is more structurally organized [18]. The presence of more complex silicate structures in the $2.0~SiO_2/Na_2O$ molar ratio activating solution, as shown in Fig. 3A, can result in an increased formation of colloidal silicate complexes that aggregate to sizes on the order of a few nanometers, which probably contribute in addition to the direct slag particle interaction to the G' and the yield stress of the suspension [18, 36]. It can also be observed that the stress eventually increases again

beyond the yield stress level with increasing strain at larger strain amplitudes, indicating the strain beyond which all structures susceptible to breakage at the yield stress level are broken. In Fig. 5D, the stress evolution in the linear deformation regime is similar for all water ratios. However, the suspension with the lowest $\rm H_2O$ content of 59 wt% in the solution reaches a higher yield stress plateau.

3.4. Suspension crosslinking and viscoelastic behaviour of the suspension

To investigate the network structure within the suspension and its LVE behaviour, frequency sweeps were conducted with angular frequencies from 100 to 0.1 rad/s in the linear regime ($\gamma=0.01$ %) [11]. Fig. 6A shows that for all ratios under investigation, G' is larger than G' over a wide frequency range (except for some of the lowest frequencies), indicating solid-like response within the time scale window of the investigated frequencies. Furthermore, a suspension with a higher SiO₂/Na₂O molar ratio developed higher G' values. This higher G' can



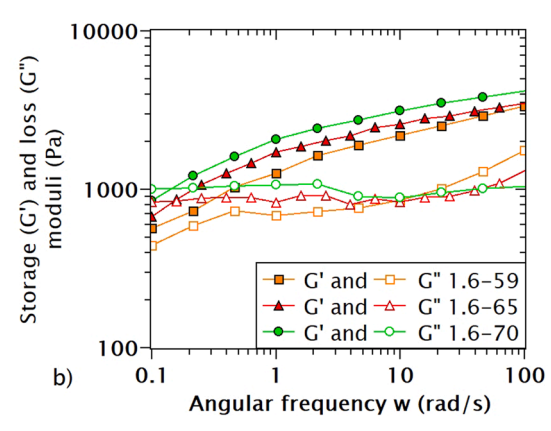


Fig. 6. The evolution of G' and G'' at various angular frequencies and a constant γ of 0.01 % for suspensions with different SiO_2/Na_2O molar ratios in (A) and different H_2O amounts in (B).

be related to a stiffer suspension, which is induced by stronger particle interactions and an increasing amount of colloidal silicate complexes from the activator (Fig. 3A), resulting in a more organised and denser network structure in the suspension [11]. A solution with a low SiO₂/-Na2O molar ratio consists mainly of silicate monomers and dimers (Fig. 3A), which resulted in a lower G', indicating a less defined network structure in the suspension. It is also clear from Fig. 6A that for all ratios at low frequencies a drop in G' and a cross-over of the G' and G" curves is observed. This indicates the presence of terminal flow behaviour [24] and a dominant viscous contribution to the LVE spectrum at these low frequencies and thus a liquid-like response at long timescales. This means that the suspension is able to (slowly) flow or creep and to follow the movement of the vane at low frequencies in order to relax [11]. Consequently, G' decreases more rapidly at low frequencies and G" gains importance. The frequency of the cross-over points of G' and G" for each sample (which is inverse related to the relaxation time) exhibit a small shift to lower frequencies when increasing the SiO₂/Na₂O molar ratio, indicating an increased relaxation time.

At high frequencies, G' exhibits a plateau value as the vane movement was too fast for the system to relax the stresses via viscous flow. This elastic plateau can be related to the suspension network density on a local scale [37], which seems to be stronger developed for a suspension with a 2.0 SiO₂/Na₂O molar ratio solution, with a higher number of colloidal silicate complexes in the activator [36]. However, Fig. 6B illustrates that also a higher amount of H2O in the suspension resulted in a G' increase, or a stiffer suspension [38] and more structural developed network. The latter might be related to the presence silanol groups from the activating solution (Fig. 2B) or a different surface charge of the slag particles, leading to a stronger interaction and slag particle floc formation due a decrease in steric and electrostatic repulsion. However, a different H₂O amount in the solution resulted in no major change to the silicate complexes (Fig. 3B), which allows to draw the conclusion that the silanol groups have little effect on the frequency dependency (Fig. 6B). In order to explain the exact nature of these results, future research is required. The G' difference between the different H2O amounts is not as large as the G' difference between the SiO2/Na2O

molar ratios (Fig. 6A). G" becomes dominant again at low frequencies, likely caused by increased repulsive forces between the particles, which is typical for gels with low solid volume fractions that show a terminal flow regime [11]. To achieve a suspension capable of being self-levelling at rest conditions, it is important to have G" dominance at low frequencies, which can be obtained by lowering the SiO₂/Na₂O ratio or by increasing the water amount in the activating solution.

3.5. Flow behaviour

The steady flow behaviour of a suspension at different shear rates, which is related to processes such as pumping or mixing, is shown in Fig. 7A and B, where the suspensions were subjected to a stepwise increase in steady state shear rate \dot{y} . At low shear rates, the stress is approximately constant and independent of the rate, and the viscosity decreases in the double logarithmic presentation with a slope of approximately -1, typical for yield stress fluids, such as concentrated non-Newtonian suspensions [24]. Similar to the stress plateau with increasing strain in the LVE data in Fig. 5C and D, the constant yield stress is the result of the physical interactions between the particles being broken down at this shear stress level [11]. When \dot{y} is further increased beyond a critical rate, the stress response of the broken down structure eventually rises above the yield stress level approaching a slope of 1 at the highest apparent rates. In this regime the flowing suspension exhibits a Newtonian-like fluid behaviour with a shear rate independent viscosity [24,39].

The samples with a higher SiO₂/Na₂O molar ratio exhibit a lower apparent viscosity when approaching the Newtonian plateau at high shear rates (Fig. 7A). This is not unexpected, as a higher degree of slag dissolution with increasing SiO₂/Na₂O molar ratio, results in a lower solid volume fraction, which leads to lower viscosity at shear rates regime beyond the yielding regime. An additional reason could be a reported plasticizing effect of the silicates in the activating solution. When increasing the SiO₂/Na₂O molar ratio, more colloidal silicate complexes from the activator diminish the particle interaction via a depletion stabilization between the particles during shearing.

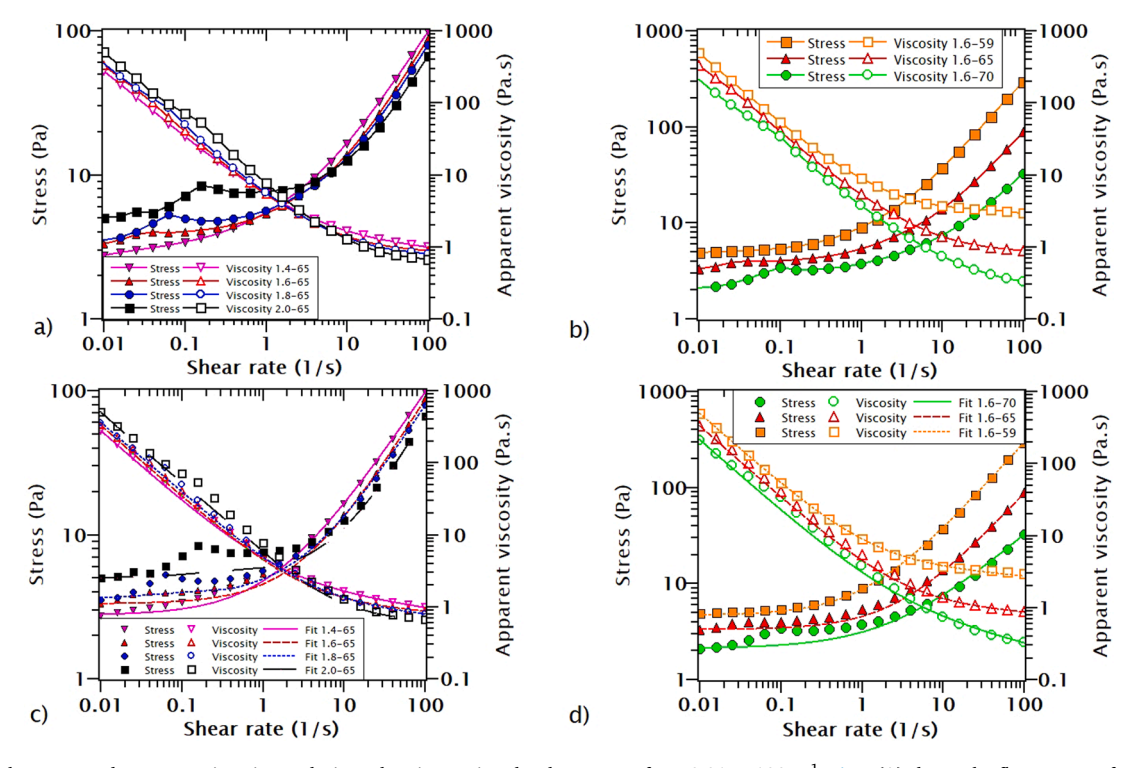


Fig. 7. (A–D) The stress and apparent viscosity evolution when increasing the shear rate \dot{y} from 0.01 to 100 s⁻¹. Fig. 7(A) shows the flow sweep of suspensions with different SiO₂/Na₂O molar ratios, while (B) shows the flow sweep of suspensions with different H₂O amounts. Panels (C) and (D) show the calculated fit.

Comparing the absolute stress and viscosity levels in the different flow regimes, it becomes clear from Fig. 7A that at low shear rates \dot{y} , a yield stress was observed for all suspensions, irrespective of the molar ratio [13]. The level of this yield stress increased when the SiO₂/Na₂O molar ratio was increased, and this is different from the trend of the viscosity level beyond the yielded regime (that dropped with increasing SiO₂/-Na₂O ratio). The decrease of volume fraction of solids with increasing SiO₂/Na₂O ratio (Table 4), result in a lower the viscosity at higher shear rates and also lead to a lower concentration of structural elements causing the yield stress. However, since the yield stress is rising, this indicates that increasing the SiO2/Na2O molar ratios must have led to a more organised structure by the combination of the increased number of colloidal silicate complexes and the flocs formed from the slag interparticle attractive forces. These become even more visible when the overall viscosity is decreased due to lower solids volume fractions. Furthermore, it is interesting to note that this more organised suspension structure goes along with the occurrence of a double yield with two distinct stress plateaus at low \dot{y} , which is in particular visible for the suspension with highest SiO₂/Na₂O molar ratio, but also slightly visible for the ratios 1.8 and 1.6. The first yield stress is situated around 5 Pa, while the second is around 7 Pa for the suspension with a SiO₂/Na₂O molar ratio of 2.0. This double yield can be related to the suspension structure, which is likely built up from different interactions, such as interparticle interactions and the interactions between the colloidal silicates and the particles, each broken down at a different stress value. The double yield is shifted to lower y when decreasing the SiO₂/Na₂O molar ratio, which indicates that the suspension structure is easier to break down.

Fig. 7B illustrates that both the apparent viscosity and the yield stress were typically higher for suspensions with a lower amount of H₂O in the activating solution. The double yielding, which can clearly be observed for the 70 wt% H₂O solution, diminishes with decreasing water content. The viscosity increase (in the regime beyond the yield stress) can be related to the higher fraction of solids present in the solution, which generally results in a higher viscosity in suspensions (Table 4) [14]. A higher solid volume fraction also resulted in the higher yield stress. Furthermore, the increase in the viscosity level at high rates was more significant over the range of H₂O variations in Fig. 7B in comparison to the viscosity increase over the SiO₂/Na₂O molar ratio range in Fig. 7A. The SiO₂/Na₂O molar ratio had only a small effect on the flow behaviour compared to the amount of H2O in the activating solution, the latter controlled the rheology under shear conditions. The viscosity in the vielded regime is therefore mainly defined by the solids volume fraction and thus the amount of H₂O, as shown in Fig. 7B. For the yield stress, a closer inspection of the oscillary data in Fig. 5C and D confirms the existence of the apparent double yielding observed in Fig. 7C and D, since both the SiO2/Na2O molar ratio of 2.0 and the 59 wt% H2O solution system exhibit a clear overshoot of the oscillatory stress with increasing strain in Fig. 5C and D.

To quantify the relevant rheological parameters, the viscosity and shear stress data was fitted with the Herschel-Bulkley model (Eqs. (1) and (2)). Using the Sum Squared Error (SSE) method, n, k, and yield stress σ_0 values for each suspension were obtained (Table 4). As shown in Fig. 7C and D, the measured values follow the trend of the fit confirming that the suspensions can indeed be described by this constitutive model. The observed double yielding is obviously not sufficiently

Table 4 The obtained k, n, and σ_0 values calculated from SSE method for the suspension made from different activating solutions.

H ₂ O (wt%)	59	70	65	65	65	65
SiO ₂ /Na ₂ O (molar ratio)	1.6	1.6	1.4	1.6	1.8	2.0
Volume solid / total volume (%)	69.5	61.9	65.3	65.2	65.2	65.1
k	3.93	1.00	1.99	1.20	1.25	0.61
n	0.93	0.74	0.84	0.92	0.89	0.99
Yield stress σ_0 (Pa)	4.91	2.10	2.76	3.31	3.65	5.05

described with the single yields stress that enters the simple Herschel-Bulkley model. It was therefore chosen to fit the lower stress plateau as application relevant yield point at low apparent shear rates, resulting in a larger deviation of the SSE for the suspension with 70 wt% H₂O and for those with a SiO₂/Na₂O molar ratio of 2.0 and 1.8. The observed increase in yield stress σ_0 when the H₂O amount decreased or SiO₂/Na₂O molar ratio increased correlates with the absolute values given in Table 4. A comparison to the independently determined yield stress from the stress plateaus and maxima of the oscillatory measurements in Fig. 5C and D confirms the obtained values of Table 4. The n values that define the slope of the viscosity curve at high shear rates are close to 1, which points to a slight shear thinning of the suspension in the observable high shear rate range [10] and a Newtonian behavior that is eventually reached at high shear rates.

3.6. The effect of the slag particles on the rheological behaviour

The aforementioned results described the rheological behaviour of the slag suspension and the effect of the activating solution chemistry on the rheology. By comparing the slag alkali-silicate suspension (slag-AS) with a suspension of inert quartz powder in the alkali-silicate solution (Qz-AS), an idea can be obtained to know to which extend the slag particle interaction forces, likely Van der Waals and electrostatic forces [39], affect the rheological behaviour in addition to the simple effect of particle volume occupation. The quartz powder is an inert material with a chemistry that differs significantly from the slag. In this case, the Qz-AS can have a different and much lower particle interaction potential compared to the slag-AS, which can result in a different rheological behaviour.

The strain amplitude sweep of the Qz suspension (Fig. 8A) shows a LVE regime of G' at low strain amplitudes, until a strain of 0.01 % is reached. Once this strain is exceeded, a strong decline in G' is measured, indicating the absence of strong particle interaction forces. This is in contrast to the slag-AS, where the slow decline of G' indicates the presence of stronger interaction forces. The oscillation stress with strain amplitude is given in Fig. 8B and shows a more gradual increase in stress when increasing the strain, in contrast to the stress plateau observed for the slag-AS (Fig. 6C). The stress at high strain amplitudes is also significantly lower (0.4 Pa) in Qz-AS compared to the slag suspension (2 Pa). The reason for this difference can be observed from the frequency sweep in Fig 8C, that shows that G' is similar to G" over the observed frequency range and that G' and G" increase with a similar slope when increasing the angular frequency. The latter is indicative for a system close to the onset of flow or jamming point when transitioning from a fluid to a weak gel (so called critical gel point). Also the absence of a plateau value of G' at high frequencies indicates that the Qz-AS has only a low network density on a local scale, typical for a critical gel of suspended particles. This is in general agreement with the volume fraction regime for model hard spherical particles, where this transition to a gel or glassy state is observed around solids volume fractions >40%. This is in contrast to the results of the slag suspension, which has a G' that becomes independent from the frequency at high frequencies, indicating the presence of a developed network density at local scale that is stronger than the one expected for a pure particle suspension at this solids concentration level. This strong difference in network strength can also be seen from the G' and G" values of the Qz-AS (Fig. 8C), that are an order of magnitude lower compared to the moduli in the slag-AS (Fig. 6).

The flow sweep results also indicate that the Qz-AS suspension is close to the jamming transition of a critical gel and show at low rates a shear thinning behaviour with the viscosity decreasing with a slope approaching -1 when increasing ý (Fig. 8D). This indicates the presence of a yield stress around 0.7 Pa, which is, however, less pronounced compared to a slag-AS (Fig. 7). This stress value is an order of magnitude larger than that of the oscillatory stress in Fig. 8B, (in the regime where a lower increase with strain was observed) indicating that Fig. 8B showed

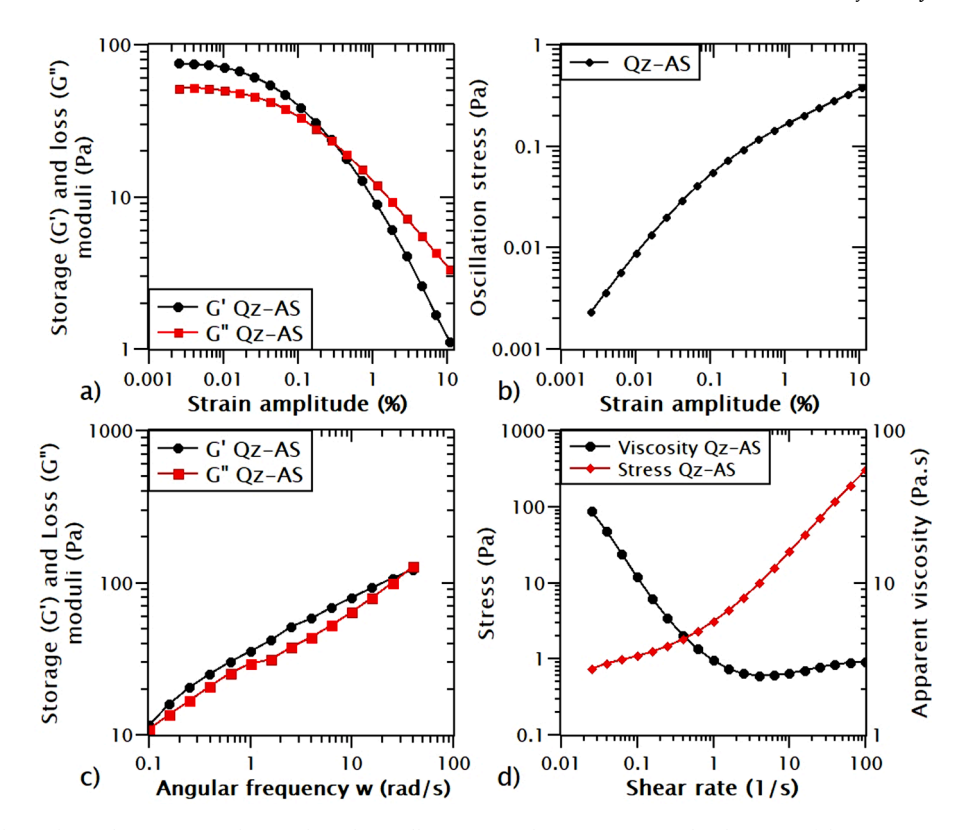


Fig. 8. (A–D). Panel(A) shows the evolution in G' and G", and (B) the oscillation stress, during a strain amplitude sweep of the Qz-AS suspension. Panel (C) shows the G' and G" of the Qz-AS suspension at different angular frequencies. Panel (D) shows the stress and viscosity when increasing the shear rate.

simply the onset of the non-linear deformation regime. A plateau value of the viscosity of 3 Pa.s is reached at a \dot{y} of 3 1/s. At high \dot{y} , a slight shear thickening behavior is measured as expected for a suspension close to the critical gel point or jamming transition. Generally, at high y, the stress and viscosity values of the Qz-AS fall in the range of the slag-AS. This is expected because the volume fraction of the Qz is similar to the slag, and at high \dot{y} all formed additionally formed network structures in the slag-AS are broken down. In principle the stress and viscosity of a suspension at high \dot{v} are determined only by the solid volume fraction (for the same activating solution SiO₂/Na₂O ratio and H₂O content). However, the viscosity and stress values at low y of the Oz-AS differ significantly from values reached in the slag-AS. A yield stress, with a value of around 5 Pa, that is measured in slag-AS, is not determined in the Qz-AS, which indicate the absence of the formation of a structural network in the Qz-AS suspension. As a result the viscosity at low y is significant lower (30 Pa.s) compared to the slag-AS (ranging from 300 to 800 Pa.s). In general, a slag-AS and a Qz-AS with a similar solid volume fraction show a different rheological behaviour, which is related to the physical interaction forces between the particles. The comparative study shows that a higher yield and viscosity is reached for the slag-AS due to more interaction forces between the slag particles . These interaction forces result in a higher network density in the suspension due to the formation of flocs, probably driven by electrostatic and Van der Waals forces, which defined the rheological behaviour of the slag-AS.

Any additional impact of the matrix fluid on interactions between the slag particles on the rheology was identified by comparing the slag-AS and Qz-AS suspension with flow sweep tests of Qz-H₂O and slag-H₂O suspensions with the same solids volume fractions. Scaling the total viscosity with the different matrix viscosities of water and the alkalisilicate solution respectively, by calculating the relative viscosity, shows for the same solids volume fractions the relative difference in influence of the fluid on the viscosity. The relative viscosity was obtained by dividing the viscosity of the suspension with the viscosity of the liquid phase μ_{S} (alkali-silicate solution or only water). The evolution

in relative viscosity with shear rate is shown Fig. 9 and indicates that all suspensions have a similar relative viscosity at high shear. This is expected as at these shear rates all suspension structures are broken down and all suspensions have similar solid and liquid volume fractions. When decreasing the shear rate, the relative viscosity of the slag-H₂O and slag-AS increases consistently, a behaviour which was less significant for Qz-H₂O. At low shear rates, the viscosity values of Qz-H₂O are unreliable as sedimentation occurred at these low rates. This effect was not visible for slag-H₂O as the latter was less susceptible to sedimentation due to its smaller D_{50} and D_{90} . Additionally, slag particles likely have significant interaction potential, which might create a stable network that decreases the sedimentation rate. Interesting to note is that the relative viscosity of the slag-H₂O at low shear rate is higher compared to the slag-

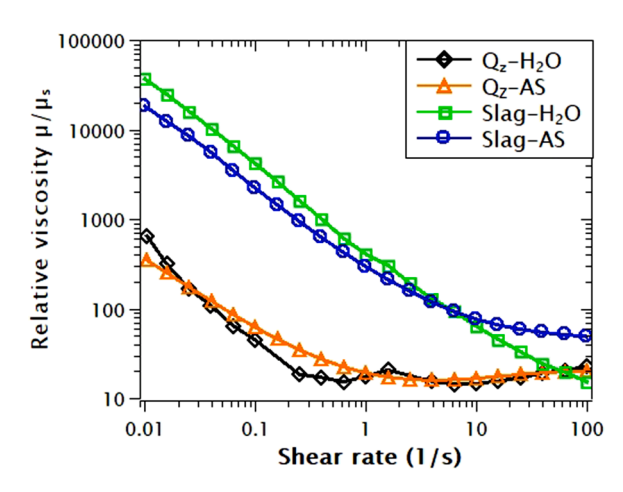


Fig. 9. The evolution in relative viscosity with shear rate of each slag-based suspension (slag-AS and slag- H_2O) and Qz-based suspension (Qz-AS and Qz- H_2O) with as liquid water or the 16-65 alkali-silicate solution.

AS, which might be related to the fact that the complex Na-silicates from the activating solution can adsorb on the surface of the slag particles, creating a plasticizing effect. The slag surface charge and the electrostatic layer around the particles can depend on the pH, which is significantly different when using an alkali-silicate solution instead of water. This can lead to a different viscosity at low shear rate. The main difference in Fig. 9 is that slag suspensions have a significantly higher relative viscosity at low rates compared to the Qz-AS and Qz-H₂O suspensions, indicating that the slag, due to its interparticle forces, significantly contributes to the rheological behaviour of the suspension at rest and at low shear rates.

Additional strain amplitude and frequency sweep experiments were conducted with the slag- H_2O and $Qz-H_2O$ suspensions, but not shown here for the sake of brevity. In $Qz-H_2O$ suspension, G" is dominant over G' and both are small (2 Pa), indicating that no elastic components were present in $Qz-H_2O$. The oscillatory tests of $Qz-H_2O$ were also affected by sedimentation, as G'<G" and due to the absence of a network structure. This led to poor data quality and the results are therefore not presented here. Some elastic contribution could still be identified for the slag- H_2O (G' dominant), indicating that the slag particle interactions can contribute to a minor extent to elasticity (G' 100 Pa) even in aqueous suspension.

4. Conclusion

An Fe-rich slag, originating from the recycling of non-ferrous scrap metal, is activated by an alkali-silicate solution to produce an inorganic polymer binder. The flow behaviour of the slag-alkali-silicate suspension depended on the alkaline solution chemistry, resulting in different flow behaviour for different SiO₂/Na₂O molar ratios. The storage modulus G' at high frequencies is practically independent of the angular frequency, indicating the presence of an organized structure in each suspension, likely formed by the attractive forces between the slag particles. When the SiO₂/Na₂O molar ratio in the activating solution is increased from 1.4 to 2.0, less hydroxide ions are available to depolymerize the silicate network. In this case, more crosslinked silicate complexes, which could form colloids, were present in the activating solution and improved the elastic properties of the suspension. The colloidal silicate complexes, and their interaction with the particles, likely contributed to an increased yield stress at low apparent shear rates. The rheological data of the suspension can be fitted with a Herschel-Bulkley model. When the amount of H₂O in the activating solution increased from 59 to 70 wt%, a slight increase in elastic properties combined with a decrease in the yield stress level was measured. The presence of silanol groups resulted in a slight increase of the elasticity of the suspension structure, but could be easily broken down. During shear, the H2O amount or solid volume fraction and the slag particle interaction force were the major factors affecting viscosity and yield stress. A comparative study between a quartz and a slag-based suspension shows that the slag interaction forces in the slag suspension contribute significantly to the yield stress. Even with the absence of any significant time dependent structural changes, such as chemical reactions, the slag suspension has a strong physical interaction between the particles which defines the rheological behaviour of the suspension. Further research can be performed on the creeprecovery behaviour and the effect of plasticizers on the rheology in order to find an applicable plasticizer.

Authors' statement

G. Beersaerts executed the conceptualisation, data curation, writing and visualisation. A. Vananroye, D. Sakellariou, C. Clasen and G. Beersaerts wrote the methdodology and the formal analysis. A. Vananroye, D. Sakellariou, C. Clasen and Y. Pontikes performed supervision and reviewing and editing.

Declaration of Competing Interest

None

Acknowledgement

The authors would like to thank Prof. Dr. ir. J. Mewis, Dr. ir. B. Schroyen and Dr. L. Kriskova for interesting discussions, ir. V. Hallet for his advice on ATR-FTIR and data fitting, and Dr. R. de Oliveira Silva and K. Duerinckx for help with the acquisition of the NMR spectra. This research falls under the scope of the SBO Cecomstruct project (nr. 140070), supported by the Flanders Agency for Innovation & Entrepreneurship (VLAIO), https://www.cecomstruct.be/, and by the Center for Resource, Recovery and Recycling (CR3). AV and CC acknowledge financial support by the Bijzonder Onderzoeksfonds KU Leuven (GOA 15/007). The authors declare that there is no conflict of interest regarding the publication of this article.

References

- S. Onisei, K. Lesage, B. Blanpain, Y. Pontikes, L. Struble, Early age microstructural transformations of an inorganic polymer made of fayalite slag, J. Am. Ceram. Soc. 98 (2015) 2269–2277, https://doi.org/10.1111/jace.13548.
- [2] Z. Huanhai, W. Xuequan, X. Zhongzi, T. Mingshu, Kinetic study on hydration of alkali-activated slag, Cem. Concr. Res. 23 (1993) 1253–1258, https://doi.org/ 10.1016/0008-8846(93)90062-F.
- [3] J. Davidovits, Geopolymer Cement. Geopolymer Cement a review, Institut Géopolymère, Saint-Quentin, France, 2013.
- [4] H. Xu, J.S.J. Van Deventer, The geopolymerisation of alumino-silicate minerals, Int. J. Miner. Process. 59 (2000) 247–266.
- [5] C. Siakati, A.P. Douvalis, P. Ziogas, A. Peys, Y. Pontikes, Impact of the solidification path of FeOx-SiO₂ slags on the resultant inorganic polymers, J. Am. Ceram. Soc. 103 (2020) 2173–2184, https://doi.org/10.1111/jace.16869.
- [6] J. Van De Sande, A. Peys, T. Hertel, H. Rahier, Y. Pontikes, Upcycling of non-ferrous metallurgy slags: identifying the most reactive slag for inorganic polymer construction materials, Resour. Conserv. Recycl. 154 (2020), 104627, https://doi.org/10.1016/j.resconrec.2019.104627.
- [7] N. Roussel, G. Ovarlez, S. Garrault, C. Brumaud, The origins of thixotropy of fresh cement pastes, Cem. Concr. Res. 42 (2012) 148–157, https://doi.org/10.1016/j. cemconres.2011.09.004.
- [8] C.A. Rees, J.L. Provis, G.C. Lukey, J.S.J. Van Deventer, Attenuated total reflectance fourier transform infrared analysis of fly ash geopolymer gel aging, Langmuir 23 (2007) 8170–8179, https://doi.org/10.1021/la700713g.
- [9] D.R. Dinger, Rheology for Ceramists, Dinger Ceramic Consulting Services, Clemson, SC, 2002.
- [10] M. Romagnoli, C. Leonelli, E. Kamse, M.L. Gualtieri, Rheology of geopolymer by DOE approach, Constr. Build. Mater. 36 (2012) 251–258, https://doi.org/10.1016/ i.conbuildmat.2012.04.122.
- [11] T.G. Mezger, Applied Rheology: with Joe Flow on Rheology Road, first ed., 2014. Anton Paar, Graz, Austria.
- [12] F. Irgens, Rheology and Non-Newtonian Fluids, Springer International, Trondheim, Norway, 2014.
- [13] M. Dinkgreve, J. Paredes, M.M. Denn, D. Bonn, On different ways of measuring "the" yield stress, J. Non-Newton. Fluid Mech. 238 (2016) 233–241, https://doi. org/10.1016/j.jnnfm.2016.11.001.
- [14] A.I. Laskar, R. Bhattacharjee, Rheology of fly-ash-based geopolymer concrete, ACI Mater. J. (2011) 108, https://doi.org/10.14359/51683263.
- [15] M.M. Alonso, S. Gismera, M.T. Blanco, M. Lanzón, F. Puertas, Alkali-activated mortars: workability and rheological behaviour, Constr. Build. Mater. 145 (2017) 576–587, https://doi.org/10.1016/j.conbuildmat.2017.04.020.
- [16] F. Puertas, C. Varga, M.M. Alonso, Rheology of alkali-activated slag pastes. Effect of the nature and concentration of the activating solution, Cem. Concr. Compos. 53 (2014) 279–288, https://doi.org/10.1016/j.cemconcomp.2014.07.012.
- [17] D.P. Bentz, C.F. Ferraris, M.A. Galler, A.S. Hansen, J.M. Guynn, Influence of particle size distributions on yield stress and viscosity of cement–fly ash pastes, Cem. Concr. Res. 42 (2012) 404–409, https://doi.org/10.1016/j. cemconres.2011.11.006.
- [18] K. Vance, A. Dakhane, G. Sant, N. Neithalath, Observations on the rheological response of alkali activated fly ash suspensions: the role of activator type and concentration, Rheol. Acta 53 (2014) 843–855, https://doi.org/10.1007/s00397-014-0793-z
- [19] L. Nachbaur, J.C. Mutin, A. Nonat, L. Choplin, Dynamic mode rheology of cement and tricalcium silicate pastes from mixing to setting, Cem. Concr. Res. 31 (2001) 183–192, https://doi.org/10.1016/S0008-8846(00)00464-6.
- [20] A. Poulesquen, F. Frizon, D. Lambertin, Rheological behaviour of alkali-activated metakaolin during geopolymerization, J. Non-Cryst. Solids 357 (2011) 3565–3571, https://doi.org/10.1016/j.jnoncrysol.2011.07.013.
- [21] A. Favier, J. Hot, G. Habert, N. Roussel, J.-B. d'Espinose de Lacaillerie, Flow properties of MK-based geopolymer pastes. A comparative study with standard

- Portland cement pastes, Soft Matter 10 (2014) 1134, https://doi.org/10.1039/
- [22] M. Palacios, F. Puertas, P. Bowen, Y.F. Houst, Effect of PCs superplasticizers on the rheological properties and hydration process of slag-blended cement pastes, J. Mater. Sci. 44 (2009) 2714–2723, https://doi.org/10.1007/s10853-009-3356-4.
- [23] M. Romagnoli, P. Sassatelli, M. Lassinantti Gualtieri, G. Tari, Rheological characterization of fly ash-based suspensions, Constr. Build. Mater. 65 (2014) 526–534, https://doi.org/10.1016/j.conbuildmat.2014.04.130.
- [24] J. Mewis, N.J. Wagner, Colloidal Suspension Rheology, Cambridge University Press, Cambridge, New York, 2012.
- [25] P.J. Swedlund, G.M. Miskelly, A.J. McQuillan, An attenuated total reflectance IR study of silicic acid adsorbed onto a ferric oxyhydroxide surface, Geochim. Cosmochim. Acta 73 (2009) 4199–4214, https://doi.org/10.1016/j. gca.2009.04.007.
- [26] C.A. Rees, J.L. Provis, G.C. Lukey, Van Deventer, S.J. Jannie, In situ ATR-FTIR study of the early stages of fly ash geopolymer gel formation, Langmuir 23 (2007) 9076–9082, https://doi.org/10.1021/la701185g.
- [27] W.K.W. Lee, J.S.J. van Deventer, Structural reorganisation of class F fly ash in alkaline silicate solutions, Colloids Surf. A 211 (2002) 49–66, https://doi.org/ 10.1016/S0927-7757(02)00237-6.
- [28] D. Dimas, I. Giannopoulou, D. Panias, Polymerization in sodium silicate solutions: a fundamental process in geopolymerization technology, J. Mater. Sci. 44 (2009) 3719–3730, https://doi.org/10.1007/s10853-009-3497-5.
- [29] J.L. Bass, G.L. Turner, Anion distributions in sodium silicate solutions. Characterization by 29 SI NMR and infrared spectroscopies, and vapor phase osmometry, J. Phys. Chem. B 101 (1997) 10638–10644, https://doi.org/10.1021/ ip9715282.
- [30] J.L. Provis, P. Duxson, G.C. Lukey, F. Separovic, W.M. Kriven, J.S.J. Van Deventer, Modeling speciation in highly concentrated alkaline silicate solutions, Ind. Eng. Chem. Res. 44 (2005) 8899–8908, https://doi.org/10.1021/ie050700i.

- [31] M.E. Simonsen, C. Sønderby, Z. Li, E.G. Søgaard, XPS and FT-IR investigation of silicate polymers, J. Mater. Sci. 44 (2009) 2079–2088, https://doi.org/10.1007/ e10853.009.3270.9
- [32] R. Dupuis, D. Gomes Rodrigues, J.-B. Champenois, R.J.-M. Pellenq, A. Poulesquen, Time resolved alkali silicate decondensation by sodium hydroxide solution, J. Phys. Mater. 3 (2020) 14012, https://doi.org/10.1088/2515-7639/ab5ce9.
- [33] G. Engelhardt, D. Michel, High-Resolution Solid-State NMR of Silicates and Zeolites, Wiley, Chichester, 1987
- [34] L.G. Engelhardt, D. Zeigan, H. Jancke, W. Wieker, D. Hoebbel, ²⁹Si-NMR-Spektroskopie an Silicatlösungen. II. Zur Abhängigkeit der Struktur der Silicatanionen in wässrigen Natriumsilicatlösungen vom Na: Si-Verhältnis, Z. Anorg, Allg. Chem. 418 (1977) 17–28.
- [35] R.K. Harris, E.K.F. Bahlmann, K. Metcalfe, E.G. Smith, Quantitative silicon-29 NMR investigations of highly concentrated high-ratio sodium silicate solutions, Magn. Reson. Chem. 31 (1993) 743–747, https://doi.org/10.1002/mrc.1260310810.
- [36] J.F. Stebbins, I. Farnan, X. Xue, The structure and dynamics of alkali silicate liquids: a view from NMR spectroscopy, Chem. Geol. 96 (1992) 371–385, https://doi.org/10.1016/0009-2541(92)90066-E.
- [37] A. Favier, J. Hot, G. Habert, E.D. Lacaillerie, N. Roussel, Rheology of geopolymer: comparative study between portland cement and metakoalin based geopolymer, Unpublished, 2013.
- [38] K.N. Pham, G. Petekidis, D. Vlassopoulos, S.U. Egelhaaf, W.C.K. Poon, P.N. Pusey, Yielding behaviour of repulsion- and attraction-dominated colloidal glasses, J. Rheol. 52 (2008) 649–676, https://doi.org/10.1122/1.2838255.
- [39] N. Roussel, A. Lemaître, R.J. Flatt, P. Coussot, Steady state flow of cement suspensions: a micromechanical state of the art, Cem. Concr. Res. 40 (2010) 77–84, https://doi.org/10.1016/j.cemconres.2009.08.026.